ACS NANO
Cite This: ACS Nano XXXX, XXX, XXX−XXX
www.acsnano.org

ARTICLE

Ultrasmall Hyperbranched Semiconducting Polymer Nanoparticles with Different Radioisotopes Labeling for Cancer Theranostics

Xuan Yi,[†] Meiyun Xu,[†] Hailin Zhou, Saisai Xiong, Rui Qian, Zhifang Chai, Li Zhao,* and Kai Yang*

State Key Laboratory of Radiation Medicine and Protection, School of Radiation Medicine and Protection & School for Radiological and Interdisciplinary Sciences (RAD-X), Collaborative Innovation Center of Radiation Medicine of Jiangsu Higher Education Institutions, Soochow University, Suzhou, Jiangsu 215123, China

Supporting Information

ABSTRACT: **Exploiting ultrasmall nanoparticles as multifunctional nanocarriers labeled with different radionuclides for tumor theranostics has attracted great attention in past few years. Herein, we develop multifunctional nanocarriers based on ultrasmall hyperbranched semiconducting polymer (HSP) nanoparticles for different radionuclides including technetium-99m (^{99m}Tc), iodine-131 (^{131}I), and iodine-125 (^{125}I) labeling. SPECT imaging of ^{99m}Tc labeled PEGylated HSP nanoparticles (HSP-PEG) exhibit a prominent accumulation in two-independent tumor models including subcutaneously xenograft and patient derived xenograft model. Impressively, 5,6-dimethylxanthenone-4-acetic acid (DMXAA), as tumor-vascular disrupting agent (VDA), significantly improves the tumor accumulation of ^{131}I labeled HSP-PEG nanoparticles, further leading to the excellent inhibition of tumor growth after intravenous injection. More importantly, SPECT imaging of ^{125}I labeled HSP-PEG indicates that ultrasmall HSP-PEG nanoparticles could be slowly excreted from the body of a mouse through urine and feces in 1 week and cause no obvious toxicity to treated mice from blood analysis and histology examinations. Our finding from the different independent tumor models SPECT imaging shows that HSP-PEG nanoparticles may act as multifunctional nanocarriers to deliver different radionuclides for monitoring the *in vivo* behaviors of nanoparticles and cancer theranostics, which will provide a strategy for cancer treatment.**

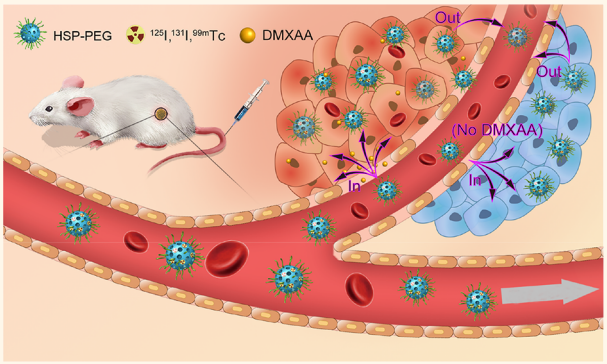

KEYWORDS: *hyperbranched semiconducting polymer, SPECT imaging, DMXAA, radioisotope therapy, metabolizable property*

Nowadays, cancer is one of the leading threats to human health.[1] Various imaging approaches including computed tomography (CT), magnetic resonance imaging (MRI), and positron emission tomography (PET)/single photon emission computed tomography (SPECT) have been widely applied in clinical diagnosis of diseases.[2] Under the guidance of imaging, a clinician will provide the right treatment for precision medicine of patients.[3−6] At present, main methods such as surgery, chemotherapy, and radiotherapy (external beam radiotherapy (RT) and internal radioisotope therapy (RIT)) have been widely used in the clinic for cancer treatments.[7−10] Although radioisotopes have been shown to have a significant advantage in both SPECT/PET imaging and RIT of tumor, how to realize the targeting delivery of radioisotopes to the tumor sites and decrease the unnecessary side effects is still a challenge.[11,12] To date, the rapid development of nanotechnology brings a nanoplatform for radionuclides targeting delivery.[13,14] Various inorganic or organic nanomaterials have been used as nanocarriers for radionuclides delivery due to the intrinsic properties of nanomaterials.[15−18] Various treatments such as photothermal therapy, photodynamic therapy, and immunotherapy have been combined with RT/RIT for improving cancer therapeutic efficiency.[19−22] Given the potential toxicity and the problem of degradation, nanomaterials based on biomolecules (e.g., protein, DNA) or ultrasmall nanoparticles have been widely acted as nanocarriers for drug and radionuclides delivery and attracted considerable attention in recent years.[23−25] Such

Received: May 9, 2018
Accepted: September 4, 2018
Published: September 5, 2018

DOI: 10.1021/acsnano.8b03514
ACS Nano XXXX, XXX, XXX−XXX

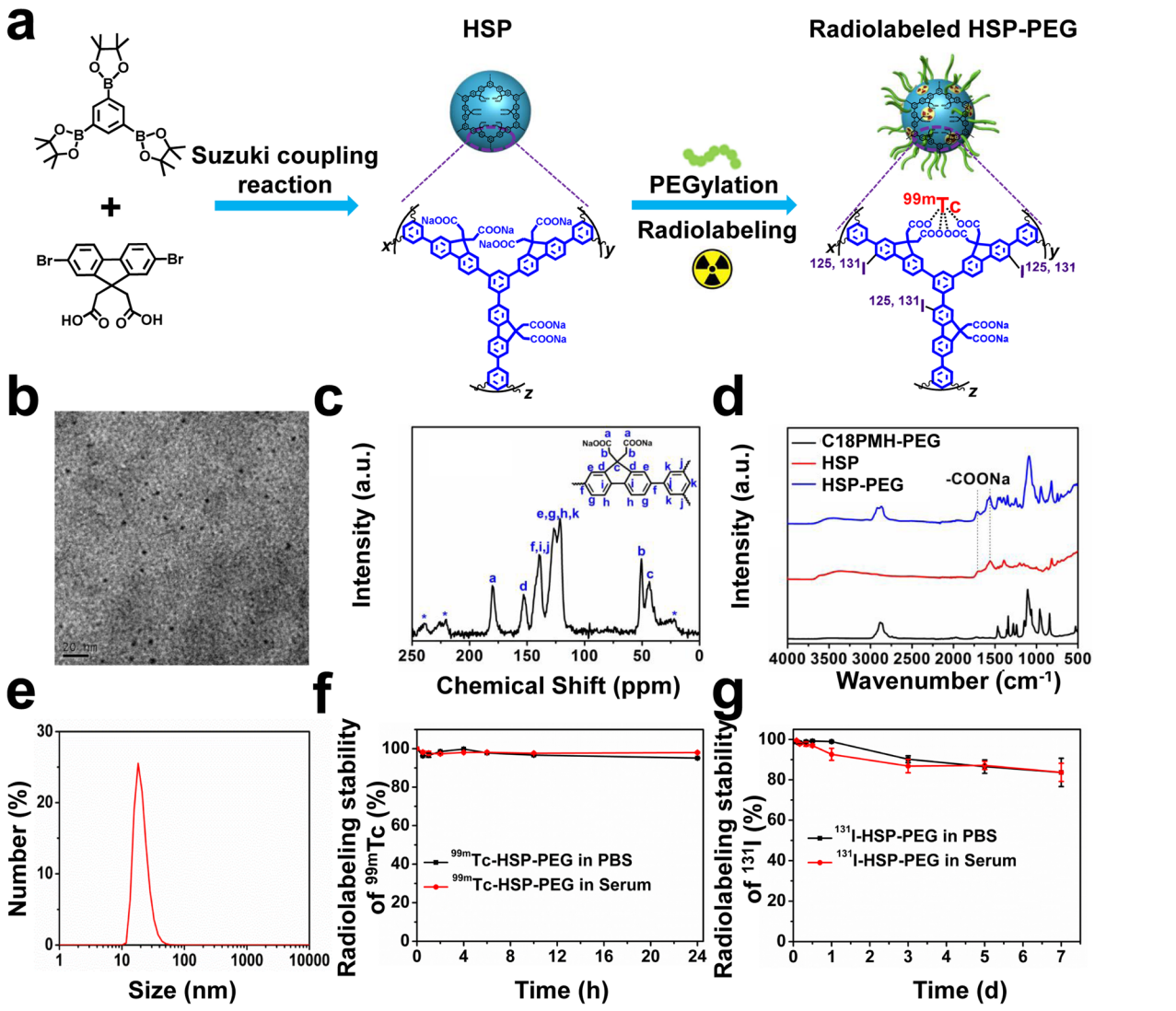

Figure 1. Preparation and characterization of radiolabeled HSP-PEG nanoparticles. (a) Schematic illustration of radiolabeled HSP-PEG nanoparticles. (b) TEM images of HSP-PEG nanoparticles. (c) The solid-state ^{13}C NMR spectroscopy of HSP nanoparticles. (d) FTIR spectra of C18-PMH-PEG, HSP nanoparticles, and HSP-PEG nanoparticles. (e) DLS data of HSP-PEG in PBS. (f,g) The radiostability of ^{99m}Tc-HSP-PEG (f) and ^{131}I-HSP-PEG (g) after incubation in PBS or serum.

strategies (the use of biomolecules or ultrasmall nanoparticles as nanocarrers) will (i) provide the excellent nanoplatform for cancer imaging and treatments, (ii) solve the biocompatibility and metabolic problems, and (iii) avoid the unnecessary side effects.[26,27] Therefore, development of a type of metabolizable nanoparticles for transportation of different radioisotopes will be attractive and practical for clinical cancer theranostics.

Semiconducting polymers with delocalized π-conjugated backbones have been widely studied in the range of biomedicine owing to their multiple advantages including unique optical properties, low toxicity, excellent biocompatibility, and easy synthesis and modification.[28−32] Until now, semiconducting polymers have been successfully used as sensitive sensors to detect biological species as imaging probes for disease diagnosis and as efficient carriers for drug delivery.[33−38] Hyperbranched semiconducting polymers (HSP) with three-dimensional dendritic architectures exhibit much larger specific surface area than their linear counterparts, possessing greater drug loading capacity.[39−41] Moreover, upon radiation, HSP are capable of diffusing the ionizing energy throughout the whole conjugated system, which alleviates the damage to chemical structure and prevents possible radiolysis.[42−45] Therefore, rationally designed HSP could serve as a potential nanocarrier of radionuclides for biomedical applications.

In this work, we developed ultrasmall HSP nanoparticles as multifunctional nanocarriers to load diagnostic radioisotope ^{99m}Tc and therapeutic radionuclide ^{131}I labeling for SPECT imaging of different independent tumor models and enhanced cancer radioisotope therapy (RIT). Ultrasmall HSP nanoparticles (~5 nm) were prepared using palladium(0)-catalyzed Suzuki coupling reaction and modified with polyethylene glycol (PEG), yielding PEGylated HSP (HSP-PEG) nanoparticles. Meanwhile, iodine isotopes could be covalently immobilized on HSP by electrophilic substitution of the protons on aromatic backbones, whereas carboxyl groups on the side chains were capable of chelating ^{99m}Tc. Taking advantage of the ultrasmall size property, HSP-PEG labeled with ^{99m}Tc could infiltrate into the tumor tissue in a short time period for accurate and seasonable SPECT imaging of different

DOI: 10.1021/acsnano.8b03514
ACS Nano XXXX, XXX, XXX−XXX

independent tumor models including 4T1 subcutaneous tumor model and subcutaneously patient-derived xenograft model. Additionally, 5,6-dimethylxanthenone-4-acetic acid (DMXAA), a representative tumor-vascular disrupting agent (VDA), enhanced the tumor uptake and prolonged the retention of ^{131}I-HSP-PEG nanoparticles in the tumor sites through the tumor vascular disruption, enabling enhanced RIT of tumor.[20] More importantly, ultrasmall HSP-PEG nanoparticles could be excreted from the major organs of mice through urine and feces uncovered by the SPECT imaging of ^{125}I labeled HSP-PEG nanoparticles. In addition, HSP-PEG nanoparticles caused no obvious toxic side effect to treated mice by the blood assay. Therefore, our study demonstrated that as-made HSP-PEG nanoparticles with ultrasmall sizes and metabolizable properties could serve as multifunctional nanocarriers to deliver different radionuclides for monitoring the *in vivo* behaviors of nanoparticles and cancer theranostics, which will provide a strategy for cancer treatment.

RESULTS AND DISCUSSION

In our study, ultrasmall hyperbranched semiconducting polymer (HSP) nanoparticles were prepared according to the published protocol with some modification.[46−48] As shown in Figure 1a, 1,3,5-tris(4,4,5,5-tetramethyl-1,3,2-dioxaborolan-2-yl) benzene and 2,2′-(2,7-dibromo-9*H*-fluorene-9,9-diyl) diacetic acid with a molar ratio of 2:3 were submitted to palladium(0)-catalyzed Suzuki coupling reaction, yielding HSP nanoparticles (Figure 1a). From the transmission electron microscopy (TEM) image, the HSP nanoparticles were uniform distribution with the size of ∼5 nm (Supporting Information (SI), Figure S1a). The chemical structure of HSP nanoparticle was characterized by solid-state ^{13}C NMR spectroscopy. The resonance signals at 180, 50, and 43 ppm in the spectrum could be attributed to −*COONa, −*CH_2COONa, and C9 of the fluorene ring (Figure 1c). The signals of the aromatic carbons were located in the range from 120 to 160 ppm.

Owing to the chemical properties, we wondered how to perform the biomedical applications of HSP. PEG grafted poly(maleic anhydride-*alt*-1-octadecene) C18-PMH-PEG was developed to modify HSP nanoparticles to improve its biocompatibility, obtaining PEGylated HSP (HSP-PEG) nanoparticles. TEM imaging showed that PEGylated HSP nanoparticles dispersed well and exhibited uniform size distribution (∼5 nm) (Figure 1b). Fourier transform infrared spectroscopy (FT-IR) was also conducted to characterize the HSP nanoparticles before and after PEG coating. It was found that HSP-PEG nanoparticles revealed two characteristic peaks at 1560 and 1710 cm^{-1} attributed to the C═O stretching vibrations of the carboxylate groups (Figure 1d). The surface charge and hydrodynamic sizes of nanoparticles were further measured by ζ potential and dynamic light scattering (DLS) measurements, respectively. The surface charge of HSP was negative owing to the deprotonation of carboxyl groups on the surface of HSP. After PEG coating, surface charge became less negative by shielding partial carboxyl (SI, Figure S2d). While the original HSP nanoparticles showed poor size distribution (PDI = 0.589) with an average size of 150 nm, which was likely induced by the aggregation of small-sized HSP nanoparticles (SI, Figure S1b), PEGylated HSP nanoparticles were monodispersed with a uniform size of 20 nm in water and showed excellent stability in different physiological solutions in one month (Figure 1e, SI, Figure S2a−c). Moreover, given the existence of the benzene ring and abundant carboxyl in the molecular formula, HSP-PEG nanoparticles could be acted on as multifunctional nanocarriers for loading of diagnostic radionuclide ^{99m}Tc with a radiolabeling yield of ∼84%, therapeutic radioisotope ^{131}I, and long half-life radionuclide ^{125}I with radiolabeling yield of ∼56%. The radiolabeling yields were similar to that of some types of radiolabeled nanoparticles.[21,49] Therefore, 4 mCi of ^{99m}Tc was mixed with HSP-PEG solution (5 mL, 0.1 mg/mL), obtaining 3.4 mCi of ^{99m}Tc-HSP-PEG for SPECT imaging of four mice. In addition, 10 mCi of ^{131}I was mixed with 0.2 mL of HSP-PEG (8 mg/mL), obtaining 5.6 mCi of ^{131}I-HSP-PEG for tumor radiotherapy. In the process of SPECT imaging and radioisotope therapy, the radionuclides should stay firmly on the probes. As expected, both radionuclide ^{99m}Tc and radioisotope ^{131}I stayed on HSP-PEG nanoparticles for a long time after incubation with phosphate buffer (PBS) and mouse serum at 37 °C (Figure 1f,g). Besides, the band gap (Eg) of HSP was estimated to be 3.08 eV on the basis of UV absorption spectrum. Such a wide band gap indicated that HSP was capable of emitting blue fluorescence, which was used for cell and tissue imaging (SI, Figure S3).[50]

Excited by the different radioisotopes labeling ability of HSP-PEG, the SPECT imaging of two-independent tumor models and *in vivo* behaviors of ultrasmall HSP-PEG nanoparticles as well as the enhanced radioisotope therapy (RIT) was conducted systematically. Before *in vivo* evaluation, we first investigated the *in vitro* cellular uptake of HSP-PEG nanoparticles. 4T1 murine breast cancer cells incubated with HSP-PEG nanoparticles for different time were obtained for flow cytometry analysis or imaged by confocal microscopy. Owing to the intrinsic fluorescence properties of HSP-PEG nanoparticles (SI, Figure S4a), the blue fluorescent signal of cells became very strong following the increase of incubating time by flow cytometry measurement (SI, Figure S4b). Meanwhile, the confocal images showed a very strong blue signal in the cytoplasm of cells under 405 nm laser excitation (SI, Figure S4c). In addition, the potential cytotoxicity of HSP-PEG nanoparticles was also measured by the methyl thiazolyl tetrazolium (MTT) assay. No obvious toxicity to the 4T1 cells was observed even at high concentration of HSP-PEG nanoparticles (≤400 μg/mL) (SI, Figure S5a). Next, the *in vitro* RIT using ^{131}I labeled HSP-PEG nanoparticles as therapeutic agents was carried out. 4T1 cells were incubated with free ^{131}I or ^{131}I labeled HSP-PEG (^{131}I-HSP-PEG) at different radioactive doses of ^{131}I for 24 h. The relative cell viabilities were also tested by MTT assay. It was found that the viabilities of cells treated with ^{131}I-HSP-PEG exhibited prominent decrease compared with that of free ^{131}I, likely owing to the increased cell uptake of ^{131}I transported by HSP-PEG nanoparticles (SI, Figure S5b). Moreover, the cytotoxicity of DMXAA used in our study had been tested on HUVEC cells. It was found that DMXAA induced obvious cytotoxicity only at a relative high concentration of 120 μg/mL (SI, Figure S5c).

We next studied the *in vivo* behaviors of HSP-PEG nanoparticles with radioisotopes labeling. First, utilizing ^{99m}Tc labeled HSP-PEG as tracers, different tumor models including 4T1 subcutaneous tumors and subcutaneously patient-derived xenograft (PDX) models were imaged by SPECT (MILabs, Utrecht, The Netherlands). From the SPECT images of 4T1 bearing mouse after intravenous (*i.v.*) injection of ^{99m}Tc labeled HSP-PEG at 30 min, we found that

DOI: 10.1021/acsnano.8b03514
ACS Nano XXXX, XXX, XXX−XXX

HSP-PEG nanoparticles distributed into the whole body of the mouse, especially in the reticuloendothelial system (RES). Afterward, the distribution of HSP-PEG nanoparticles in heart and lung were decreased following blood circulation, while the radioactivity of the bladder became very strong, likely owing to the fact that ultrasmall HSP-PEG nanoparticles could be excreted from the body through urine. The results further excluded the possibility of released ^{99m}Tc from HSP-PEG nanoparticles by comparing with the SPECT imaging of mice injected with free ^{99m}Tc (SI, Figure S6). Moreover, we used filter paper chromatography to analyze the radioactive component in urine of the mice treated with ^{99m}Tc-HSP-PEG nanoparticles. From the data, we found that free ^{99m}Tc was concentrated in regions 6 and 7, while ^{99m}Tc-HSP-PEG was concentrated in region 1. The radioactive component in the urine stayed in region 1, suggesting that most of them should be ^{99m}Tc-HSP-PEG nanoparticles (SI, Figure S7). In addition, we observed some black dots in urine of mice treated with HSP-PEG nanoparticles through the TEM assay (SI, Figure S8). Both of the above evidence indicated that HSP-PEG could be excreted through urine. Additionally, ^{99m}Tc labeled HSP-PEG exhibited high tumor uptake via enhanced permeability and retention (EPR) effect (Figure 2a and SI, Figure S9a). Besides, PDX models have been considered to be more clinically relevant tumor models. Prostate tumors from human patient were implanted into the immune-compromising mice. After 15 days of implantation, PDX models of mice were *i.v.* injected with ^{99m}Tc labeled HSP-PEG nanoparticles and imaged by SPECT. Similar to 4T1 tumor models, ^{99m}Tc labeled HSP-PEG nanoparticles exhibited high PDX tumor accumulation (Figure 2b and SI, Figure S9b). Therefore, our as-made HSP-PEG nanoparticles could act as excellent theranostics agents for imaging of different tumor models.

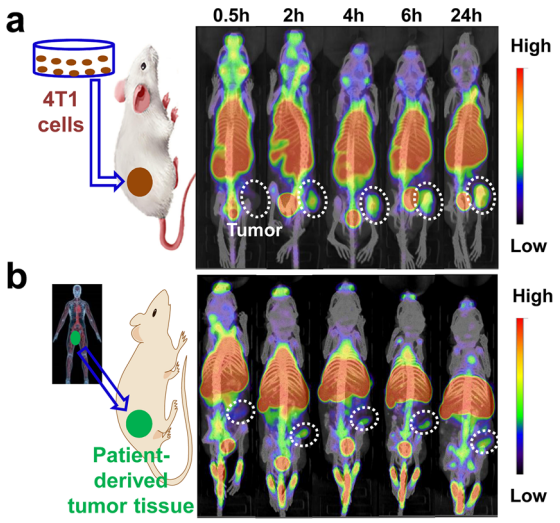

Figure 2. SPECT/CT imaging of two different tumor models. SPECT imaging of 4T1-tumor-bearing mice (a) and patient-derived prostate tumor tissue-bearing mice (b) after *i.v.* injection with ^{99m}Tc-HSP-PEG taken at the different time points post injection.

Motivated by high tumor uptake of ^{99m}Tc labeled HSP-PEG nanoparticles, we next studied the *in vivo* tumor RIT using radioisotope ^{131}I labeled HSP-PEG (^{131}I-HSP-PEG) as therapeutic agents (Figure 3a). According to the literature,[20] DMAXX is widely used to induce the damage of tumor vascular and cause the formation of congestion which is beneficial for the accumulation of nanoparticles or drug in the tumor sites. In this work, after DMXAA treatment, the vascular destruction of tumor tissue was investigated through immunofluorescent staining of CD31. Compared with the intact and sequential vessels in normal tumor, the continuity of the vessels was broken after DMXAA injection. Strong blue fluorescence signal from HSP-PEG nanoparticles was observed in the DMXAA treated tumor tissue (Figure 3b). Next, the blood circulation and biodistribution of ^{131}I-HSP-PEG in 4T1 bearing mice were carefully tested in our study. Blood samples from mice treated with ^{131}I-HSP-PEG nanoparticles were collected and measured the radioactivity by gamma counter at various time points post injection (*p.i.*). The results showed that the blood circulation of ^{131}I-HSP-PEG nanoparticles followed a classical two-compartment model. The first and second phase blood circulation half-lives were measured to be 0.32 ± 0.05 h and 14.17 ± 1.33 h, respectively (Figure 3c). Such long-time blood circulation was attributed to well surface coating, which could assist the nanoparticles to escape the phagocytosis of macrophage in RES and enhance tumor accumulation. Besides, we also investigated the biodistribution of ^{131}I-HSP-PEG and DMXAA plus ^{131}I-HSP-PEG nanoparticles after *i.v.* injection. It was found that both ^{131}I-HSP-PEG and DMXAA plus ^{131}I-HSP-PEG nanoparticles exhibited high tumor accumulation. Importantly, we found that DMAXX could increase the tumor uptake of ^{131}I-HSP-PEG nanoparticles. The tumor uptake of ^{131}I-HSP-PEG nanoparticles was up to 5.14 ± 0.65% ID/g at the presence of DMAXX (12 mg/kg), while the ^{131}I-HSP-PEG alone exhibited 2.99 ± 0.39% ID/g of tumor uptake, which was significantly lower than that of DMXAA plus ^{131}I-HSP-PEG nanoparticles (p = 0.00787) (Figure 3d). After 72 h of injection, the retained radioactivity in the tumor sites of mice injected with ^{131}I-HSP-PEG was measured to be 3.27 ± 0.20% ID/g, which was significantly higher than the tumor accumulation of ^{131}I-HSP-PEG nanoparticles without DMXAA treatment (1.58 ± 0.13% ID/g, p = 0.00027) (Figure 3d). Moreover, compared with the undesired biodistribution of ^{131}I-HSP nanoparticles owing to the aggregation of HSP in mice blood and phagocytosis by reticuloendothelial system, the biodistribution of ^{131}I-HSP-PEG was much better for biomedical application (SI, Figure S10).

Gamma imaging (Kodak, FX Pro) was also used for observing the *in vivo* behavior of ^{131}I-HSP-PEG with or without DMXAA treatment. As showed in SI, Figure S5, while the images of mice treated with ^{131}I-HSP-PEG or DMXAA plus ^{131}I-HSP-PEG uncovered no obvious difference at 2 h post injection (*p.i.*), mice treated with DMXAA plus ^{131}I-HSP-PEG exhibited very stronger radioactive signal in the tumor sites than that of ^{131}I-HSP-PEG at 72 h *p.i.*. More importantly, the radioactivity of all of mice was decreased significantly after 72 h of injection, likely owing to that ultrasmall size of HSP-PEG nanoparticles could be excreted from the body of mice (SI, Figure S11). The results further uncovered that DMXAA could significantly increase the tumor uptake of HSP-PEG nanoparticles and keep the nanoparticles in the tumor sites for a long time, which was better for tumor nuclear imaging and RIT treatments.

Encouraged by the enhanced tumor accumulation of ^{131}I-HSP-PEG, we next used ^{131}I-HSP-PEG nanoparticles as therapeutic agents for *in vivo* tumor RIT with the help of DMAXX. 4T1 bearing mice were randomly assigned to seven

DOI: 10.1021/acsnano.8b03514
ACS Nano XXXX, XXX, XXX−XXX

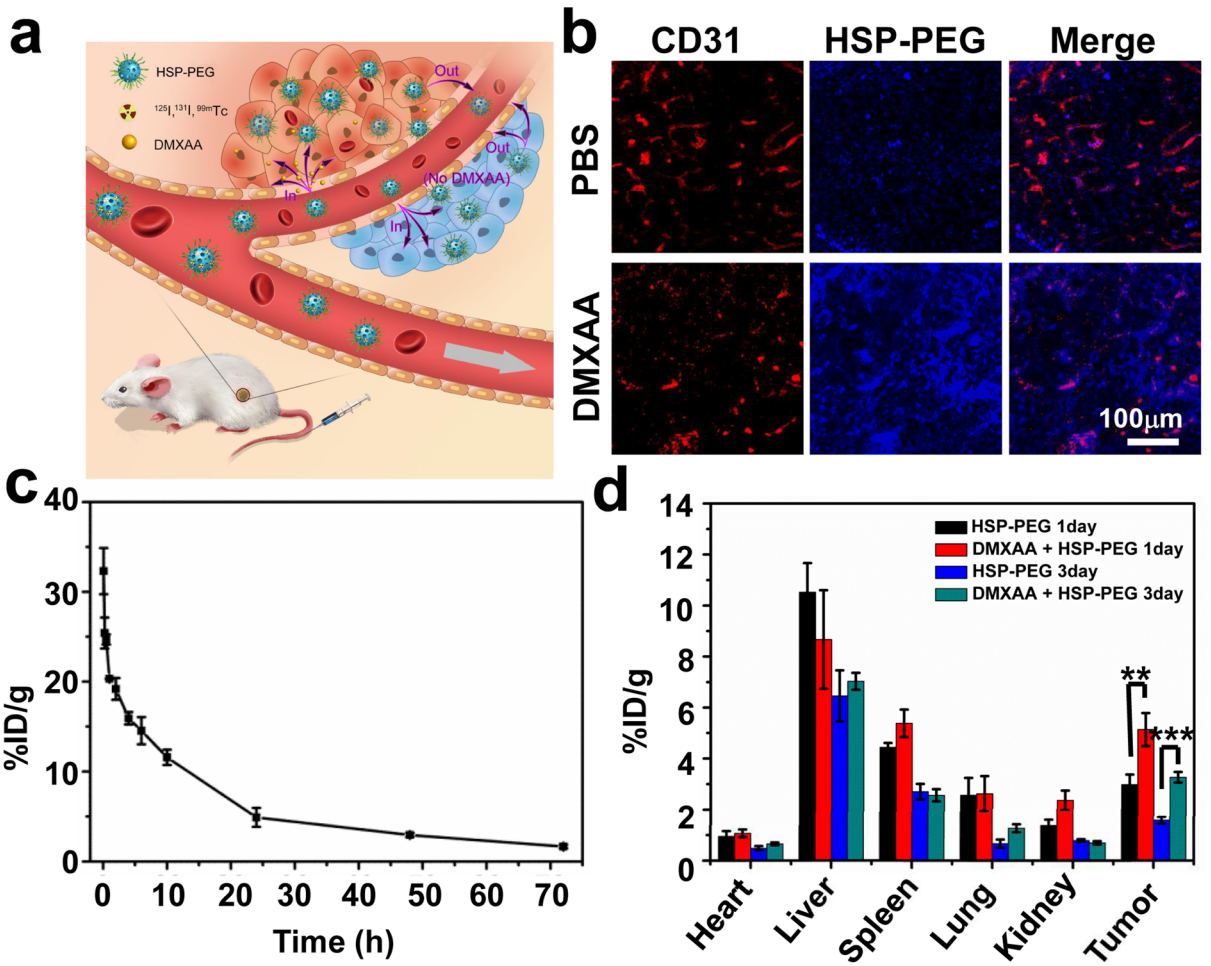

Figure 3. *In vivo* behaviors of ^{131}I labeled HSP-PEG with or without DMXAA injection. (a) Schematic illustration of increased tumor uptake and long tumor retention of radioisotope labeled HSP-PEG with the help of DMXAA. (b) Destructive tumor vessels and then enhanced tumor uptake of HSP-PEG after DMXAA treatment. (c) The blood circulation of ^{131}I-HSP-PEG. (d) The biodistribution of ^{131}I-HSP-PEG measured at 1 and 3 d post injection with or without DMXAA. Statistical analysis was performed using the Student's two-tailed *t* test (**P* < 0.05, ***P* < 0.01, ****P* < 0.001).

groups (five mice per group). The groups included (i) mice *i.v.* injected with PBS, (ii) mice *i.v.* injected with HSP-PEG (10 mg/kg), (iii) mice *i.v.* injected with the mixture of DMXAA and free ^{131}I (12 mg/kg of DMXAA and 300 μCi per mouse of ^{131}I), (iv) mice *i.v.* injected with ^{131}I-HSP-PEG, and (v) mice *i.v.* injected with DMXAA plus ^{131}I-HSP-PEG. Nanoparticles or free drugs were injected two times at day 0 and day 7 throughout the treatment. To compare the therapeutic efficiency between one injection and two injections, we added two groups: (vi) mice *i.v.* injected with ^{131}I-HSP-PEG (600 μCi per mouse of ^{131}I) at 0 day and (vii) mice *i.v.* injected with DMXAA plus ^{131}I-HSP-PEG (12 mg/kg of DMXAA and 600 μCi per mouse of ^{131}I) at 0 day. The tumor sizes and the mice weight were measured every other day. It was found that the tumors of mice in groups (i) and (ii) showed almost similar growth speed, suggesting that HSP-PEG did not affect the tumor growth (Figure 4a). In addition, free DMXAA and ^{131}I at low dose also did not affect the tumor growth. On the contrary, ^{131}I-HSP-PEG remarkably enhanced the therapeutic efficiency of ^{131}I compared with that of free DMXAA and ^{131}I, achieving the obvious inhibition of tumor growth. It was because the HSP-PEG nanoparticles could greatly enhance tumor uptake of ^{131}I. Although 50% of tumor growth was inhibited for the ^{131}I-HSP-PEG nanoparticles treated group, DMXAA plus ^{131}I-HSP-PEG could inhibit almost 80% of tumor growth, indicating that DMXAA plus ^{131}I-HSP-PEG exhibited excellent therapeutic efficiency of cancer (p = 000268). Moreover, the therapeutic efficiency of two injections were better than that of injection of all radiopharmaceuticals at one time owing to the half-life of radionuclide ^{131}I (Figure 4a). After 14 days of treatment, the tumors were collected for taking a picture, further confirming the excellent therapeutic efficiency of ^{131}I-HSP-PEG nanoparticles with the help of DMXAA (Figure 4b).

Besides, Hematoxylin & Eosin (H&E) staining and terminal deoxynucleotidyl transferase dUTP nick end labeling (TUNEL) assay were conducted to investigate morphologic change and apoptosis of cancer cells in different treated groups. As shown in Figure 4c, we found that a large number of erythrocytes, which exist only in the blood vessels, dispersed in the whole tumor tissue for DMXAA treated mice (Figure 4c). However, such phenomenon was not observed in other groups. The results further confirmed that DMAXX could induce the tumor vascular damage and enhance erythrocytes accumulation in the tumor sites. Meanwhile, tumors of mice in each group were collected for TUNEL staining. From observing the brown or black cells in the slices, we found that tumors of mice in group (iv) and (v) showed the higher level of cell apoptosis

DOI: 10.1021/acsnano.8b03514
ACS Nano XXXX, XXX, XXX−XXX

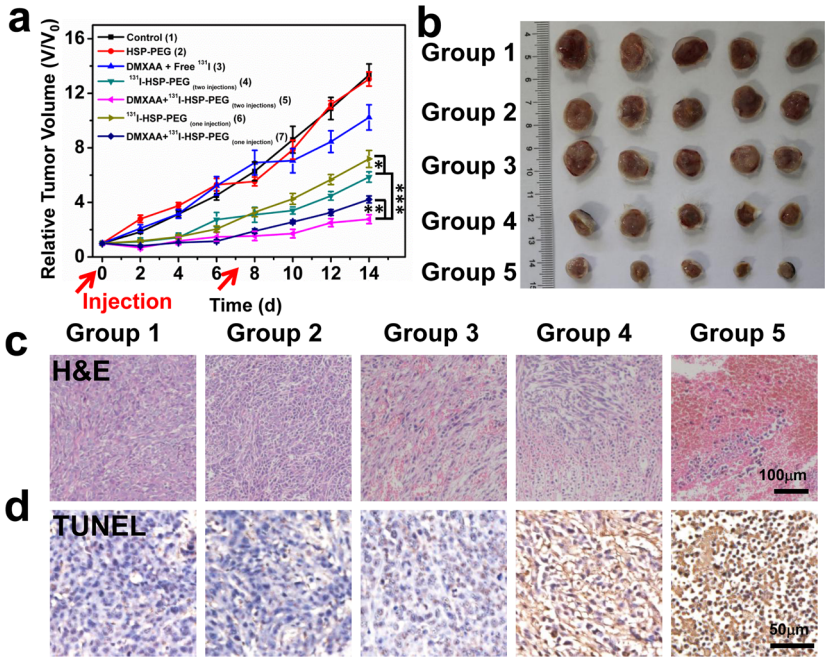

Figure 4. *In vivo* enhanced radioisotope therapy based on ^{131}I-HSP-PEG plus DMXAA. (a) Tumor growth curves of mice with different treatments. Group 1: PBS. Group 2: HSP-PEG (10 mg/kg at 0, 7 day). Group 3: DMXAA and free ^{131}I (12 mg/kg of DMXAA and 300 μCi of ^{131}I per mouse at 0, 7 day). Group 4: ^{131}I-HSP-PEG (300 μCi of ^{131}I per mouse at 0, 7 day). Group 5: DMXAA plus ^{131}I-HSP-PEG (12 mg/kg of DMXAA and 300 μCi of ^{131}I per mouse at 0, 7 day). Group 6: ^{131}I-HSP-PEG (600 μCi of ^{131}I per mouse at 0 day). Group 7: DMXAA plus ^{131}I-HSP-PEG (12 mg/kg of DMXAA and 600 μCi of ^{131}I per mouse at 0 day). Five mice were used for each group. The tumor volumes were normalized to their initial sizes. (b) The respective photos of the tumor in each group after 14 days treatment. (c,d) Micrographs of H&E (c) and TUNEL (d) stained tumor slices from mice with different treatments collected 3 days after the first treatment. Statistical analysis was performed using the Student's two-tailed *t* test (*P < 0.05, **P < 0.01, ***P < 0.001).

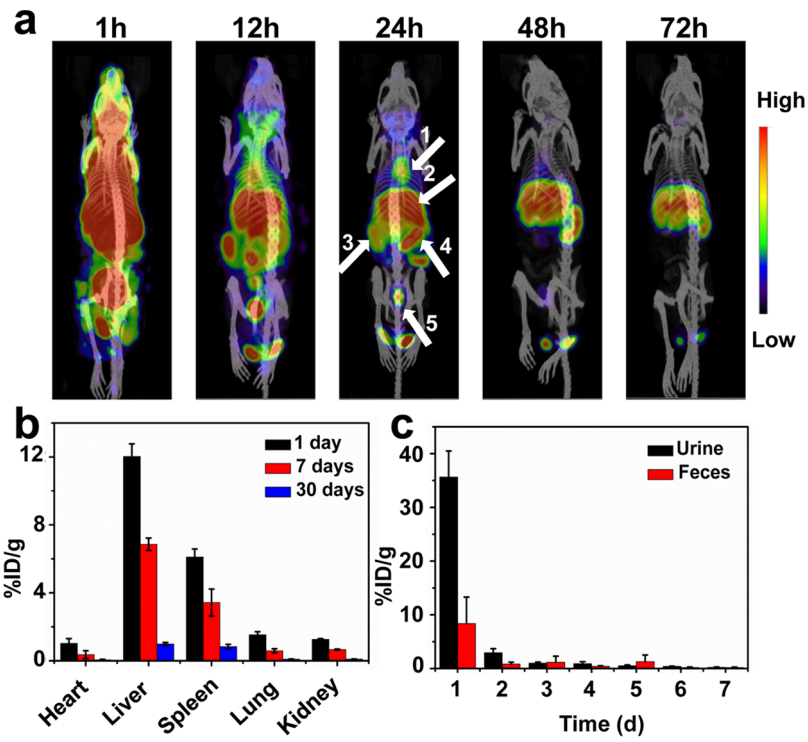

Figure 5. *In vivo* metabolism of ^{125}I-HSP-PEG. (a) SPECT/CT imaging of the mice injected ^{125}I-HSP-PEG in 3 days (white arrow 1 for heart, 2 for liver, 3 for kidney, 4 for spleen, and 5 for bladder). (b) The biodistribution of ^{125}I-HSP-PEG measured at 1, 7, and 30 days post injection. (c) Radioactive quantification of the urine and feces collected every day from the healthy mice injected ^{125}I-HSP-PEG in a week.

than control groups, suggesting that RIT could significantly induce the apoptosis of cancer cells (Figure 4d). It is noteworthy that DMXAA plus ^{131}I-HSP-PEG induced more serious apoptosis than that of ^{131}I-HSP-PEG, further

DOI: 10.1021/acsnano.8b03514
ACS Nano XXXX, XXX, XXX−XXX

suggesting the increased tumor accumulation and retention of the ^{131}I-HSP-PEG in the presence of DMXAA (Figure 4d). Our results clearly demonstrated that the therapeutic efficiency of RIT could be further enhanced through coinjection of radiolabeled ultrasmall organic conjugated nanoparticles and VDA.

In our experiment process, the body weights of the mice in all groups showed no obvious change (SI, Figure S12). We next systematically investigated the *in vivo* metabolism and potential toxicity of HSP-PEG nanoparticles. For metabolism investigation, radioisotope ^{125}I labeled HSP-PEG nanoparticles were *i.v.* injected into healthy mice (10 mg/kg of HSP-PEG corresponding 300 μCi of ^{125}I). The SPECT imaging was used to observe visually the *in vivo* biodistribution of HSP-PEG nanoparticles in the whole body of a mouse. As shown in Figure 5a, ^{125}I-HSP-PEG nanoparticles gradually dispersed into a majority of the organ and were excreted from the major organs except the liver and spleen after 72 h of injection. Most of ^{125}I-HSP-PEG nanoparticles were observed in the kidney and bladder, demonstrating that ^{125}I-HSP-PEG nanoparticles could be excreted through urine. To further ensure the metabolic pathways of ^{125}I-HSP-PEG nanoparticles, the major organs, urine, and feces were collected for gamma counter measurement of the radioactivity. The results revealed that HSP-PEG nanoparticles with ultrasmall sizes could be excreted thoroughly from the bodies of mice after 30 days of injection (Figure 5b,c). Moreover, most of nanoparticles were excreted through urine, which matched with the data of SPECT imaging (Figure 5c). For the reasons of the excretion of HSP-PEG nanoparticles through urine, we had concluded: (1) Our prepared HSP-PEG nanoparticles were 10−40 nm in size as measured by DLS. The smaller ones could be excreted quickly through the kidneys, while the bigger ones can stay in the blood for a longer time.[11,51] (2) The core of HSP-PEG was about 5 nm, and the hydrodynamic size of HSP-PEG was ∼20 nm. It was found that PEG coating increased the hydrodynamic size of HSP nanoparticles. However, PEG was flexible and could be folded.[52,53]

Next, compared with the control group, blood biochemistry including a series of the liver/kidney function markers were measured to be normal (SI, Figure S13a−c), suggesting no obvious hepatic and kidney disorder induced by HSP-PEG nanoparticles at the dose of 10 mg/kg. Additionally, a complete blood panel analysis was also carried out. The obtained data stayed in the normal ranges of the healthy mice (SI, Figure S13d−k). Meanwhile, the major organs of mice were collected at days 1, 7, and 30 for H&E staining. Compared with the healthy mice, neither noticeable morphologic change of cells nor inflammatory exudation were observed (SI, Figure S14). Moreover, to estimate the possible off-site tissue damage using ^{131}I-HSP-PEG as a nanocarrier, we collected the major organs of mice in groups 1 and 5 at days 1 and 15 for H&E staining. No necrosis or inflammation was observed (SI, Figure S15). Therefore, our synthesized HSP-PEG with different radioisotope (^{99m}Tc, ^{131}I, and ^{125}I) labeling could be developed for cancer theranostics with high biosafety.

CONCLUSIONS

In summary, HSP nanoparticles were synthesized by using a palladium(0)-catalyzed Suzuki coupling reaction, which had an average size of ∼5 nm from TEM imaging, and then noncovalently functionalized with C18-PMH-PEG, yielding HSP-PEG nanoparticles. Solid-state ^{13}C NMR spectroscopy and infrared spectrometry were used to confirm chemical structure of HSP. The obtained HSP-PEG nanoparticles could be labeled with different radioisotope such as ^{99m}Tc, ^{131}I, and ^{125}I ^{99m}Tc-HSP-PEG nanoparticles and could be used as smart SPECT imaging tracers for imaging of different tumor models including a 4T1 subcutaneous tumor model and a subcutaneously patient-derived xenograft model. Moreover, the ^{131}I-HSP-PEG could be used as an effective radiopharmaceutical for cancer treatment. DMXAA could enhance the tumor accumulation of ^{131}I-HSP-PEG and prolong their retention in the tumor site by inducing the vascular disruption. Owing to the higher and longer radiation dose in the tumor region, the tumor grown could be inhibited significantly by inducing a wide range of cell apoptosis in the tumor tissue. More importantly, SPECT imaging using ^{125}I labeled HSP-PEG as tracers could be used to monitor the *in vivo* behaviors and the metabolism of ultrasmall nanoparticles (∼5 nm), demonstrating that HSP-PEG nanoparticles could be excreted from the body in a month without inducing obvious toxicity to treated mice. Therefore, we developed ultrasmall HSP-PEG nanoparticles as multifunctional nanoagents for cancer theranostics, providing a strategy for cancer treatments and further promoting the biomedical applications of nanomaterials.

EXPERIMENTAL METHODS

Synthesis of HSP. The monomers, 2,2′-(2,7-dibromo-9*H*-fluorene-9,9-diyl) diacetic acid and 1,3,5-tris(4,4,5,5-tetramethyl-1,3,2-dioxaborolan-2-yl) benzene, were synthesized according to the methods reported previously.[46−48] 1,3,5-Tris(4,4,5,5-tetramethyl-1,3,2-dioxaborolan-2-yl)benzene (308.9 mg, 0.76 mmol) and 2,2′-(2,7-dibromo-9*H*-fluorene-9,9-diyl)diacetic acid (500 mg, 1.14 mmol) were dissolved in DMF (50 mL) and then bubbled with nitrogen for 30 min. Next, Pd(PPh3)4 (50 mg, 0,04 mmol) was added quickly into the mixture followed by injection of degassed 1 M Na_2CO_3 solution (5 mL). The reaction was conducted under nitrogen with rapid stirring at 90 °C for 24 h and then at 120 °C for 72 h. After being cooled down to room temperature, the suspension was centrifuged at 4000 rpm for 30 min and the precipitate was washed with DMF 5 times to remove unreacted monomers and small molecular impurities. The resulting solid was dialyzed against water and then freeze-dried to give HSP as a pale-yellow powder (202 mg).

Synthesis of PEGylated HSP Nanoparticles. The obtained HSP nanoparticles were noncovalently functionalized with C18-PMH-terminated PEG (C18-PMH-PEG), which was synthesized according to our published protocols.[19] Briefly, 200 mg of C18-PMH-PEG dissolved in 1 mL of DI water was added into 10 mL of HSP solution (2 mg/mL) under sonication for 1.5 h and then stirred overnight. Finally, the reacted solution was centrfuged at 14800 rpm for 30 min to remove the precipitate and collected the supernates for purification. The yield of PEGylated HSP nanoparticles was stored in 4 °C for the next experiments.

Radioisotope Labeling. To perform ^{99m}Tc labeling, 4 mCi of ^{99m}Tc, HSP-PEG solution (5 mL, 0.1 mg/mL), and stannous chloride solved in 0.1 M HCl (200 μL, 5 mg/mL) were mixed and strirred for 1 h. ^{99m}Tc labeled HSP-PEG nanoparticles were then obtained after being purified by ultrafiltration three times. Moreover, HSP-PEG was labeled with radionuclide iodine using an iodogen-coating method (a standard electrophilic substitution reaction). In brief, 10 mCi of ^{125}I or ^{131}I and 0.2 mL of HSP-PEG (8 mg/mL) were added into 1 mL of an EP tube which was coated with Iodogen. The mixture was then reacted for 30 min at room temperature. Unbonded ^{125}I or ^{131}I was removed by centrifugation.

***In Vitro* Experiments.** To investigate cellular uptake of HSP-PEG nanoparticles, 4T1 cells preseeded in 6-well plates at a density of 2×10^5 cells/well were incubated with 100 μg/mL of HSP-PEG nanoparticles. After incubation for different periods (1, 6, 12, and

DOI: 10.1021/acsnano.8b03514
ACS Nano XXXX, XXX, XXX−XXX

24 h), cells were washed with PBS three times and imaged by confocal fluorescence microscope (OLYMPUS). Meanwhile, cells were also collected for flow cytometry assay under 405 nm laser excitation.

For the *in vitro* cytotoxicity assay, the preincubated cells into 96-well plates at a density of 8000 cells per well were added with different concentrations of HSP-PEG nanoparticles, free DMXAA, free ^{131}I, or ^{131}I-HSP-PEG, respectively. After incubation of 24 h, the cell viabilities were measured by MTT assay.

SPECT/CT Imaging. The protocols of animal experiments were approved by the Soochow University Laboratory Animal Center. Preparation of the 4T1 tumor model could follow our published protocols.[7] For the PDX modal preparation, we first obtained the tumor tissue from the patients suffering prostatic cancer in Suzhou Municipal Hospital after getting informed consent. Afterward, the fresh prostatic tumor tissue was cut into pieces (~2−4 mm) in a sterile dish and then implanted onto the back of each nude mouse under general anesthesia using forceps. The skin incision was closed using an absorbable suture. All experiments were conducted in compliance with all relevant ethical regulations.[54] For SPECT/CT imaging, mice injected with ^{99m}Tc-HSP-PEG at the radioactivitive dose of 800 μCi per mouse or ^{125}I-HSP-PEG at the radioactivitive dose of 500 μCi per mouse were anesthetized and put on the bed of the SPECT imaging system for taking the SPECT/CT imaging of the whole body at appointed time points *p.i.*.

Blood Circulation and Biodistribution. To investige the blood circulation of HSP-PEG nanoparticles, blood from mice *i.v.* injected with ^{131}I-HSP-PEG (50 μCi of ^{131}I per mouse corresponding to 10 mg/kg of HSP-PEG) was collected at appointed time points *p.i.* and then weighed and measured the radioactivity by the gamma counter (LB211, Berthold Technologies Gmbh & Co. KG). In addition, mice bearing 4T1 tumors were *i.v.* injected with ^{131}I-HSP-PEG or DMXAA plus ^{131}I-HSP-PEG (12 mg/kg of DMXAA per mouse) and sacrificed at 24 h *p.i.* Major organs were collected, weighed, and measured the radioactivity by the gamma counter.

***In Vivo* Tumor Therapy.** To evaluate the *in vivo* tumor therapeutic efficiency, tumors of mice were randomly assigned to five groups (five mice per group) including (1) PBS, (2) HSP-PEG (10 mg/kg), (3) the mixture of free DMXAA and ^{131}I, (4) ^{131}I-HSP-PEG, and (5) the mixture of DMXAA and ^{131}I-HSP-PEG (12 mg/kg of DMXAA, 300 μCi of ^{131}I). The treatments were conducted two times at days 0 and 7. The tumor volumes and the body weights of mice in all groups were monitored every other day. The tumors in each group were dissected after 3 days after first injection and fixed in 10% formaldehyde for H&E staining and TUNEL staining.

Blood Analysis and Histology Examinations. The blood analysis and histology examinations could follow our previously published protocols.[19]

ASSOCIATED CONTENT

Supporting Information

This material is available free of charge on the Web site The Supporting Information is available free of charge on the ACS Publications website at DOI: 10.1021/acsnano.8b03514.

Additional analytical figures (PDF)

AUTHOR INFORMATION

Corresponding Authors

*E-mail: kyang@suda.edu.cn.
*E-mail: lizhao@suda.edu.cn.

ORCID

Kai Yang: 0000-0002-6670-1024

Author Contributions

†These authors contributed equally to this work

Notes

The authors declare no competing financial interest.

ACKNOWLEDGMENTS

This work was partially supported by National Natural Science Foundation of China (81471716, 31600805), the National Natural Science Foundation of Jiangsu Province (BK20160329), Postgraduate Research & Practice Innovation Program of Jiangsu Province (KYCX17_2016), and a Project Funded by the Priority Academic Program Development of Jiangsu Higher Education Institutions (PAPD).

REFERENCES

(1) Islami, F.; Goding Sauer, A.; Miller, K. D.; Siegel, R. L.; Fedewa, S. A.; Jacobs, E. J.; McCullough, M. L.; Patel, A. V.; Ma, J.; Soerjomataram, I.; Flanders, W. D.; Brawley, O. W.; Gapstur, S. M.; Jemal, A. Proportion and Number of Cancer Cases and Deaths Attributable to Potentially Modifiable Risk Factors in the United States. *Ca-Cancer J. Clin.* **2018**, *68*, 31−54.

(2) Zhen, X.; Feng, X.; Xie, C.; Zheng, Y.; Pu, K. Surface Engineering of Semiconducting Polymer Nanoparticles for Amplified Photoacoustic Imaging. *Biomaterials* **2017**, *127*, 97−106.

(3) Ljubimova, J. Y.; Sun, T.; Mashouf, L.; Ljubimov, A. V.; Israel, L. L.; Ljubimov, V. A.; Falahatian, V.; Holler, E. Covalent Nano Delivery Systems for Selective Imaging and Treatment of Brain Tumors. *Adv. Drug Delivery Rev.* **2017**, *113*, 177−200.

(4) Xu, C.; Chen, F.; Valdovinos, H. F.; Jiang, D.; Goel, S.; Yu, B.; Sun, H.; Barnhart, T. E.; Moon, J. J.; Cai, W. Bacteria-Like Mesoporous Silica-Coated Gold Nanorods for Positron Emission Tomography and Photoacoustic Imaging-Guided Chemo-Photothermal Combined Therapy. *Biomaterials* **2018**, *165*, 56−65.

(5) Wu, C.; Chiu, D. T. Highly Fluorescent Semiconducting Polymer Dots for Biology and Medicine. *Angew. Chem., Int. Ed.* **2013**, *52*, 3086−3109.

(6) Feng, L.; Zhu, C.; Yuan, H.; Liu, L.; Lv, F.; Wang, S. Conjugated Polymer Nanoparticles: Preparation, Properties, Functionalization and Biological Applications. *Chem. Soc. Rev.* **2013**, *42*, 6620−6633.

(7) Yi, X.; Chen, L.; Chen, J.; Maiti, D.; Chai, Z.; Liu, Z.; Yang, K. Biomimetic Copper Sulfide for Chemo-Radiotherapy: Enhanced Uptake and Reduced Efflux of Nanoparticles for Tumor Cells under Ionizing Radiation. *Adv. Funct. Mater.* **2018**, *28*, 1705161.

(8) Yan, J.; He, W.; Yan, S.; Niu, F.; Liu, T.; Ma, B.; Shao, Y.; Yan, Y.; Yang, G.; Lu, W.; Du, Y.; Lei, B.; Ma, P. X. Self-Assembled Peptide−Lanthanide Nanoclusters for Safe Tumor Therapy: Overcoming and Utilizing Biological Barriers to Peptide Drug Delivery. *ACS Nano* **2018**, *12*, 2017−2026.

(9) Cai, Y.; Liang, P.; Tang, Q.; Yang, X.; Si, W.; Huang, W.; Zhang, Q.; Dong, X. Diketopyrrolopyrrole−Triphenylamine Organic Nanoparticles as Multifunctional Reagents for Photoacoustic Imaging-Guided Photodynamic/Photothermal Synergistic Tumor Therapy. *ACS Nano* **2017**, *11*, 1054−1063.

(10) Ji, T.; Lang, J.; Wang, J.; Cai, R.; Zhang, Y.; Qi, F.; Zhang, L.; Zhao, X.; Wu, W.; Hao, J.; Qin, Z.; Zhao, Y.; Nie, G. Designing Liposomes to Suppress Extracellular Matrix Expression to Enhance Drug Penetration and Pancreatic Tumor Therapy. *ACS Nano* **2017**, *11*, 8668−8678.

(11) Cheng, L.; Jiang, D.; Kamkaew, A.; Valdovinos, H. F.; Im, H. J.; Feng, L.; England, C. G.; Goel, S.; Barnhart, T. E.; Liu, Z.; Cai, W. Renal-Clearable PEGylated Porphyrin Nanoparticles for Image-Guided Photodynamic Cancer Therapy. *Adv. Funct. Mater.* **2017**, *27*, 1702928.

(12) Ni, D.; Jiang, D.; Ehlerding, E. B.; Huang, P.; Cai, W. Radiolabeling Silica-Based Nanoparticles *via* Coordination Chemistry: Basic Principles, Strategies, and Applications. *Acc. Chem. Res.* **2018**, *51*, 778−788.

(13) Goel, S.; England, C. G.; Chen, F.; Cai, W. Positron Emission Tomography and Nanotechnology: a Dynamic Duo for Cancer Theranostics. *Adv. Drug Delivery Rev.* **2017**, *113*, 157−176.

(14) Fan, W.; Yung, B.; Huang, P.; Chen, X. Nanotechnology for Multimodal Synergistic Cancer Therapy. *Chem. Rev.* **2017**, *117*, 13566−13638.

DOI: 10.1021/acsnano.8b03514
ACS Nano XXXX, XXX, XXX−XXX

(15) Shen, S.; Jiang, D.; Cheng, L.; Chao, Y.; Nie, K.; Dong, Z.; Kutyreff, C. J.; Engle, J. W.; Huang, P.; Cai, W.; Liu, Z. Renal-Clearable Ultrasmall Coordination Polymer Nanodots for Chelator-Free ^{64}Cu-Labeling and Imaging-Guided Enhanced Radiotherapy of Cancer. *ACS Nano* **2017**, *11*, 9103−9111.
(16) Zhang, J.; Niu, G.; Lang, L.; Li, F.; Fan, X.; Yan, X.; Yao, S.; Yan, W.; Huo, L.; Chen, L.; Li, Z.; Zhu, Z.; Chen, X. Clinical Translation of A Dual Integrin $\alpha v\beta 3$−and Gastrin-Releasing Peptide Receptor−Targeting PET Radiotracer, ^{68}Ga-BBN-RGD. *J. Nucl. Med.* **2017**, *58*, 228−234.
(17) Liu, Z.; Huang, J.; Dong, C.; Cui, L.; Jin, X.; Jia, B.; Zhu, Z.; Li, F.; Wang, F. ^{99m}Tc-Labeled RGD-BBN Peptide for Small-Animal SPECT/CT of Lung Carcinoma. *Mol. Pharmaceutics* **2012**, *9*, 1409−1417.
(18) Liu, S.; Jia, B.; Qiao, R.; Yang, Z.; Yu, Z.; Liu, Z.; Liu, K.; Shi, J.; Ouyang, H.; Wang, F.; Gao, M. A Novel Type of Dual-Modality Molecular Probe for MR and Nuclear Imaging of Tumor: Preparation, Characterization and *in vivo* Application. *Mol. Pharmaceutics* **2009**, *6*, 1074−1082.
(19) Yi, X.; Yang, K.; Liang, C.; Zhong, X.; Ning, P.; Song, G.; Wang, D.; Ge, C.; Chen, C.; Chai, Z.; Liu, Z. Imaging-Guided Combined Photothermal and Radiotherapy to Treat Subcutaneous and Metastatic Tumors Using Iodine-131-Doped Copper Sulfide Nanoparticles. *Adv. Funct. Mater.* **2015**, *25*, 4689−4699.
(20) Satterlee, A. B.; Rojas, J. D.; Dayton, P. A.; Huang, L. Enhancing Nanoparticle Accumulation and Retention in Desmoplastic Tumors *via* Vascular Disruption for Internal Radiation Therapy. *Theranostics* **2017**, *7*, 253−269.
(21) Zhu, G.; Lynn, G. M.; Jacobson, O.; Chen, K.; Liu, Y.; Zhang, H.; Ma, Y.; Zhang, F.; Tian, R.; Ni, Q.; Cheng, S.; Wang, Z.; Lu, N.; Yung, B. C.; Wang, Z.; Lang, L.; Fu, X.; Jin, A.; Weiss, I. D.; Vishwasrao, H.; Niu, G.; Shroff, H.; Klinman, D. M.; Seder, R. A.; Chen, X. Albumin/vaccine Nanocomplexes that Assemble *in vivo* for Combination Cancer Immunotherapy. *Nat. Commun.* **2017**, *8*, 1954.
(22) Veeravagu, A.; Liu, Z.; Niu, G.; Chen, K.; Jia, B.; Cai, W.; Jin, C.; Hsu, A. R.; Connolly, A. J.; Tse, V.; Wang, F.; Chen, X. Integrin $\alpha v\beta 3$-targeted Radioimmunotherapy of Glioblastoma Multiforme. *Clin. Cancer Res.* **2008**, *14*, 7330−7339.
(23) Tian, L.; Chen, Q.; Yi, X.; Wang, G.; Chen, J.; Ning, P.; Yang, K.; Liu, Z. Radionuclide I-131 Labeled Albumin-Paclitaxel Nanoparticles for Synergistic Combined Chemo-Radioisotope Therapy of Cancer. *Theranostics* **2017**, *7*, 614−623.
(24) Yu, X.; Li, A.; Zhao, C.; Yang, K.; Chen, X.; Li, W. Ultrasmall Semimetal Nanoparticles of Bismuth for Dual-modal Computed Tomography/Photoacoustic Imaging and Synergistic Thermoradiotherapy. *ACS Nano* **2017**, *11*, 3990−4001.
(25) Jiang, Y.; Upputuri, P. K.; Xie, C.; Lyu, Y.; Zhang, L.; Xiong, Q.; Pramanik, M.; Pu, K. Broadband Absorbing Semiconducting Polymer Nanoparticles for Photoacoustic Imaging in Second Near-infrared Window. *Nano Lett.* **2017**, *17*, 4964−4969.
(26) Zhou, Z.; Wang, Y.; Yan, Y.; Zhang, Q.; Cheng, Y. Dendrimer-templated Ultrasmall and Multifunctional Photothermal Agents for Efficient Tumor Ablation. *ACS Nano* **2016**, *10*, 4863−4872.
(27) Tang, S.; Chen, M.; Zheng, N. Sub-10-nm Pd Nanosheets With Renal Clearance for Efficient Near-infrared Photothermal Cancer Therapy. *Small* **2014**, *10*, 3139−3144.
(28) Miao, Q.; Xie, C.; Zhen, X.; Lyu, Y.; Duan, H.; Liu, X.; Jokerst, J. V.; Pu, K. Molecular Afterglow Imaging with Bright, Biodegradable Polymer Nanoparticles. *Nat. Biotechnol.* **2017**, *35*, 1102−1110.
(29) Zhu, H.; Fang, Y.; Miao, Q.; Qi, X.; Ding, D.; Chen, P.; Pu, K. Regulating Near-Infrared Photodynamic Properties of Semiconducting Polymer Nanotheranostics for Optimized Cancer Therapy. *ACS Nano* **2017**, *11*, 8998−9009.
(30) Jiang, Y.; Pu, K. Multimodal Biophotonics of Semiconducting Polymer Nanoparticles. *Acc. Chem. Res.* **2018**, *51*, 1840−1849.
(31) Wu, W.; Bazan, G. C.; Liu, B. Conjugated-Polymer-Amplified Sensing, Imaging, and Therapy. *Chem.* **2017**, *2*, 760−790.
(32) Li, J.; Rao, J.; Pu, K. Recent Progress on Semiconducting Polymer Nanoparticles for Molecular Imaging and Cancer Phototherapy. *Biomaterials* **2018**, *155*, 217−235.
(33) Liu, B.; Bazan, G. C. Methods for Strand-specific DNA Detection with Cationic Conjugated Polymers Suitable for Incorporation into DNA Chips and Microarrays. *Proc. Natl. Acad. Sci. U. S. A.* **2005**, *102*, 589−593.
(34) Lyu, Y.; Zeng, J. F.; Jiang, Y. Y.; Zhen, X.; Wang, T.; Qiu, S. S.; Lou, X.; Gao, M. Y.; Pu, K. Y. Enhancing Both Biodegradability and Efficacy of Semiconducting Polymer Nanoparticles for Photoacoustic Imaging and Photothermal Therapy. *ACS Nano* **2018**, *12*, 1801−1810.
(35) Pu, K.; Shuhendler, A. J.; Jokerst, J. V.; Mei, J.; Gambhir, S. S.; Bao, Z.; Rao, J. Semiconducting Polymer Nanoparticles as Photoacoustic Molecular Imaging Probes in Living Mice. *Nat. Nanotechnol.* **2014**, *9*, 233−239.
(36) Cao, Y.; Wu, Y.; Wang, G.; Yi, J.; Yu, C.; Huang, Y.; Sun, L.; Bao, Y.; Li, Y. Near-infrared Conjugated Polymers for Photoacoustic Imaging-guided Photothermal/chemo Combination Therapy. *J. Mater. Chem. B* **2017**, *5*, 5479−5487.
(37) Li, J.; Xie, C.; Huang, J.; Jiang, Y.; Miao, Q.; Pu, K. Semiconducting Polymer Nanoenzymes with Photothermic Activity for Enhanced Cancer Therapy. *Angew. Chem., Int. Ed.* **2018**, *57*, 3995−3998.
(38) Lyu, Y.; Cui, D.; Sun, H.; Miao, Y.; Duan, H.; Pu, K. Dendronized Semiconducting Polymer as Photothermal Nanocarrier for Remote Activation of Gene Expression. *Angew. Chem., Int. Ed.* **2017**, *56*, 9155−9159.
(39) Wei, X.; Luo, Q.; Sun, L.; Li, X.; Zhu, H.; Guan, P.; Wu, M.; Luo, K.; Gong, Q. Enzyme-and pH-sensitive Branched Polymer−Doxorubicin Conjugate-Based Nanoscale Drug Delivery System for Cancer Therapy. *ACS Appl. Mater. Interfaces* **2016**, *8*, 11765−11778.
(40) Sun, L.; Li, X.; Wei, X.; Luo, Q.; Guan, P.; Wu, M.; Zhu, H.; Luo, K.; Gong, Q. Stimuli-responsive Biodegradable Hyperbranched Polymer−Gadolinium Conjugates as Efficient and Biocompatible Nanoscale Magnetic Resonance Imaging Contrast Agents. *ACS Appl. Mater. Interfaces* **2016**, *8*, 10499−10512.
(41) Zhuang, Y.; Deng, H.; Su, Y.; He, L.; Wang, R.; Tong, G.; He, D.; Zhu, X. Aptamer-functionalized and Backbone Redox-Responsive Hyperbranched Polymer for Targeted Drug Delivery in Cancer Therapy. *Biomacromolecules* **2016**, *17*, 2050−2062.
(42) Yik, B. J.; Guo, M.; Kwon, Y.; Goodson, T., III New Approaches for Energy Storage with Hyperbranched Polymers. *J. Phys. Chem. C* **2017**, *121*, 7108−7122.
(43) Wu, X.; Li, H.; Xu, B.; Tong, H.; Wang, L. Solution-dispersed Porous Hyperbranched Conjugated Polymer Nanoparticles for Fluorescent Sensing of TNT with Enhanced Sensitivity. *Polym. Chem.* **2014**, *5*, 4521−4525.
(44) Hu, R.; Lam, J. W.; Tang, B. Z. Hyperbranched Conjugated Polymers. *Encyclopedia of Polymeric Nanomaterials* **2015**, 971−977.
(45) Han, X.; Xu, M.; Yang, S.; Qian, J.; Hua, D. Acetylcysteine-functionalized Microporous Conjugated Polymers for Potential Separation of Uranium from Radioactive Effluents. *J. Mater. Chem. A* **2017**, *5*, 5123−5128.
(46) Bao, B.; Yuwen, L.; Zhan, X.; Wang, L. Water-Soluble Hyperbranched Polyelectrolytes with High Fluorescence Quantum Yield: Facile Synthesis and Selective Chemosensor for Hg^{2+} and Cu^{2+} Ions. *J. Polym. Sci., Part A: Polym. Chem.* **2010**, *48*, 3431−3439.
(47) Qin, C.; Wu, X.; Gao, B.; Tong, H.; Wang, L. Amino Acid-functionalized Polyfluorene as a Water-soluble Hg^{2+} Chemosensor with High Solubility and High Photoluminescence Quantum Yield. *Macromolecules* **2009**, *42*, 5427−5429.
(48) Qin, C.; Wu, X.; Tong, H.; Wang, L. High Solubility and Photoluminescence Quantum Yield Water-Soluble Polyfluorenes with Dendronized Amino Acid Side Chains: Synthesis, Photophysical, and Metal Ion Sensing Properties. *J. Mater. Chem.* **2010**, *20*, 7957−7964.
(49) Zhong, X.; Yang, K.; Dong, Z.; Yi, X.; Wang, Y.; Ge, C.; Zhao, Y.; Liu, Z. Polydopamine as a Biocompatible Multifunctional

DOI: 10.1021/acsnano.8b03514
ACS Nano XXXX, XXX, XXX−XXX

Nanocarrier for Combined Radioisotope Therapy and Chemotherapy of Cancer. *Adv. Funct. Mater.* **2015**, *25*, 7327−7336.
(50) Wang, X.; Sui, D.; Huang, M.; Jiang, Y. Highly Effective Hydration of Olefins Using a Wool-Palladium Complex as a Catalyst. *Polym. Adv. Technol.* **2006**, *17*, 163−167.
(51) Jiang, X.; Zhang, S.; Ren, F.; Chen, L.; Zeng, J.; Zhu, M.; Cheng, Z.; Gao, M.; Li, Z. Ultra-Small Magnetic $CuFeSe_2$ Ternary Nanocrystals for Multimodal Imaging Guided Photothermal Therapy of Cancer. *ACS Nano* **2017**, *11*, 5633−5645.
(52) Liu, K.; Dong, L.; Xu, Y.; Yan, X.; Li, F.; Lu, Y.; Tao, W.; Peng, H.; Wu, Y.; Su, Y.; Ling, D.; He, T.; Qian, H.; Yu, S.-H. Stable Gadolinium Based Nanoscale Lyophilized Injection for Enhanced MR Angiography with Efficient Renal Clearance. *Biomaterials* **2018**, *158*, 74−85.
(53) Gómez-Vallejo, V.; Puigivila, M.; Plaza-García, S.; Szczupak, B.; Piñol, R.; Murillo, J. L.; Sorribas, V.; Lou, G.; Veintemillas, S.; Ramos-Cabrer, P.; Llop, J.; Millán, A. PEG-Copolymer-Coated Iron Oxide Nanoparticles that Avoid the Reticuloendothelial System and Act as Kidney MRI Contrast Agents. *Nanoscale* **2018**, *10*, 14153−14164.
(54) Inoue, T.; Terada, N.; Kobayashi, T.; Ogawa, O. Patient-Derived Xenografts as *in vivo* Models for Research in Urological Malignancies. *Nat. Rev. Urol.* **2017**, *14*, 267−283.

DOI: 10.1021/acsnano.8b03514
ACS Nano XXXX, XXX, XXX−XXX